

# High-Speed One-Photon 3D Nanolithography Using Controlled Initiator Depletion and Inhibitor Transport

Shih-Hsin Hsu, Teng Chi, Jinwoo Kim, Paul Somers, Bryan W. Boudouris, Xianfan Xu, and Liang Pan\*

Additive manufacturing of sophisticated 3D nanoscale objects commonly uses femtosecond lasers to photopolymerize a light-sensitive resin using multi-photon absorption. This nonlinear process provides high accuracy and flexibility in advanced 3D fabrication; however, it typically has limited throughput and high cost. This work makes use of a one-photon-based dosage-nonlinearity to fabricate 3D nanostructures, demonstrating a cost-effective method for 3D nanolithography using a low-cost 405 nm continuous-wave diode laser. This dosage-nonlinearity is achieved by using controlled depletion of photo-initiation species in an environment containing inhibiting species. By controlling multiple competing processes, the undesired dose accumulation outside the writing voxel is stopped, and thereby this method creates a confined writing voxel in space. A multiphysics model is developed to numerically study the one-photon nonlinear photopolymerization process, which is compared with experimental results.

penetration thereby creating a patterning zone confined to the top-most layer of the resin bath. A mechanical recoating procedure is performed for forming a new resin layer before each projection. Layered 3D objects are then created by repeating dynamic 2D optical patterns onto each layer of resin.<sup>[10]</sup> To avoid the slow-down by the recoating step, a fluorinated oil has been used as a mobile liquid interface to maintain a constant supply of fresh resin for continuous fabrication.<sup>[11]</sup> Yet another way to improve the printing speed, the continuous liquid interface production, adds a dead zone of polymerization beneath the writing zone which allows continuous refill of fresh resin without the need for a dedicated recoating step.<sup>[12]</sup> A typical approach is to use a gas-permeable window to create an oxygen-rich dead

zone near the window and use oxygen to inhibit radical polymerization. An alternative approach is to photochemically generate inhibiting agents, defining the dead zone by using a second light beam.<sup>[13]</sup> Recently, a reverse algorithm of computed tomography imaging was used to spatially control the dosage of illumination and create 3D parts using fast volumetric illuminations.<sup>[14,15]</sup>

Laser scanning methods can write fine features at the nanoscale. Two-photon lithography uses nonlinear excitation of photo-responsive materials to polymerize confined 3D regions (voxels).<sup>[16–19]</sup> It typically requires a femtosecond laser operating at a near IR wavelength and scanning the voxel location inside material to create 3D shapes. When using high numerical aperture objectives, two-photon lithography can reliably produce submicron features beyond the diffraction limit. Inspired by stimulated-emission depletion, the writing voxel size can be further reduced by another depletion light and has reliably been demonstrated for nanoscale patterning at about 20–30 nm.<sup>[20–23]</sup> Despite the advantages of its high patterning resolution, conventional two-photon lithography still has a relatively higher tool cost than projection  $\mu$ SL. Recent research used a spatial-temporal focusing effect to perform multiphoton projection to enhance the process throughput and successfully build millimeter-sized 3D parts with sub-micron features.<sup>[23,24]</sup> Multiphoton printing throughput has been significantly scaled up through the use of beam splitting techniques for printing with multiple foci.<sup>[25–27]</sup> However, the multiphoton absorption process requires femtosecond lasers as light sources which represents a significant tool cost for mass production.<sup>[23,24]</sup> Instead,

## 1. Introduction

Additive manufacturing patterns 3D parts for rapid prototyping and low-volume production in many technological areas.<sup>[1–4]</sup> It proliferates with several distinct technologies and is capable of building objects covering a wide range of materials and feature dimensions.<sup>[5–9]</sup> Among them, photopolymerization is a common approach to create features at the microscale in a light-sensitive resin bath.<sup>[2]</sup> Because of its processing accuracy and flexibility, photopolymerization can create complicated 3D shapes by the projection of dynamic optical fields or fast scanning of a focused laser beam. One-photon projection printing methods, such as the micro-stereolithography ( $\mu$ SL) method and its derivatives print objects in a layer-by-layer manner, adding inert photo absorbers to the resins to limit the light

S.-H. Hsu, J. Kim, P. Somers, X. Xu, L. Pan  
School of Mechanical Engineering and Birck Nanotechnology Center  
Purdue University  
West Lafayette, IN 47907, USA  
E-mail: liangpan@purdue.edu

T. Chi, B. W. Boudouris  
Charles D. Davidson School of Chemical Engineering and Department  
of Chemistry  
Purdue University  
West Lafayette, IN 47907, USA

 The ORCID identification number(s) for the author(s) of this article can be found under <https://doi.org/10.1002/adom.202102262>.

DOI: 10.1002/adom.202102262

a one-photon process can work with the diode laser, operating at a power of milliwatt level or lower, which provides a low-cost alternative to print 3D nanostructures. By allowing dissolved oxygen to refill around a writing voxel excited by lower power, researchers have written 3D nanostructures using a continuous-wave laser at a writing speed up to  $10 \mu\text{m s}^{-1}$ .<sup>[28–30]</sup> Other researchers used photo-induced radicals to produce the inhibition effect near the voxel to create 3D structures.<sup>[31,32]</sup> Furthermore, other one-photon based processes, such as photo-thermal initiations, are also demonstrated to locally activate polymerization at the voxels.<sup>[33–35]</sup> The above one-photon nonlinear printing processes still require lasers with high peak powers, writing at low speeds, or coordination of multiple light sources. Here, we report a high-speed 3D nanolithography method using a one-photon nonlinear polymerization process that operates at a low peak laser power for high-speed writing. By designing the molar concentration of photoinitiator to be the same order as the inhibiting species, we used a new nonlinear effect arise from the depletion of initiation species to stop undesired dose accumulation outside the writing voxel to spatially and temporally control the activation of initiating together with the transport of inhibiting species to perform 3D nanoscale patterning at scanning speeds of 100s of  $\mu\text{m s}^{-1}$  using an average laser power of a few milliwatts.

## 2. Results and Discussion

A home-built system with a compact diode laser operating at 405 nm wavelength (shown in Figure S1 in the Supporting Information) is used to conduct the laser direct-write experiments. As shown in Figure 1a, the system scans a focused laser beam into the resin bath and selectively polymerizes the resin to create 3D structures, anchored onto a substrate, with the assistance of inhibition by controlling multiple competing processes.

To achieve a Schwarzschild-type dosage-nonlinear response, the concentrations and components of the photocurable resin are designed based on the free radical polymerization reactions as shown in Figure 1b and the chemical structures of the key components are shown in Figure 1c. The concentration of the

photoinitiator, phenylbis(2,4,6-trimethylbenzoyl)phosphine oxide (BAPO; Sigma-Aldrich), is chosen to be on the same order of magnitude as the dissolved oxygen concentration, around  $1 \times 10^{-3} \text{ M}$  in the resin.<sup>[15]</sup> When the initiator molecules BAPO (In) in the resin absorb photon energy ( $h\nu$ ) from the laser, they are excited and undergo photo-cleavage to generate active radicals ( $R\cdot$ ). The active radicals attach to the monomer (M), triethylene glycol dimethacrylate (TEGDMA; Sigma-Aldrich) and launch a propagation reaction to form the polymeric networks. Typically, in this free-radical polymerization process, the conversion of the monomer is determined by the accumulative number of photons absorbed (exposure dose), disregarding the intensity and exposure time of the light, which yields a linear process. However, once the concentration of photoinitiators has declined to a similar level to that of the dissolved oxygen, a highly nonlinear response begins to arise due to the competing effects between inhibition of oxygen and polymer chain growth. When low-intensity light propagates in the resin, the radicals generated are quickly consumed by inhibition species, such as the dissolved oxygen and the 4-methoxyphenol (MEHQ, also known as a polymerization retarder), as the inhibition process is several orders faster than polymerization based on their reaction nature, which prevents polymerization.<sup>[29–31,33,34]</sup> Due to the low concentration of initiator, the excited initiating radicals can be depleted by the inhibiting species and forms a spatially defined writing voxel. When the light intensity is increased to photo-cleave most of the initiators inside the voxel in a short period (such as several or a few tens of microseconds), the local inhibiting species are then promptly consumed such that the chain growth process overwhelms the inhibition process to complete polymerization in the rest of the period. In addition, the photoabsorber (Sudan I) in the resin may also absorb the light and locally increases the temperature to assist the writing process.<sup>[36]</sup> Meanwhile, at the onset of polymerization at the voxel location, radicals initiated outside the voxel would be quickly consumed by inhibiting molecules to prevent undesired polymerization, and the inhibiting molecule concentration can slowly recover by diffusion to maintain the existing inhibition process.

Fast temporal modulation of the laser intensity is employed to improve the pattern uniformity, by controlling the competition

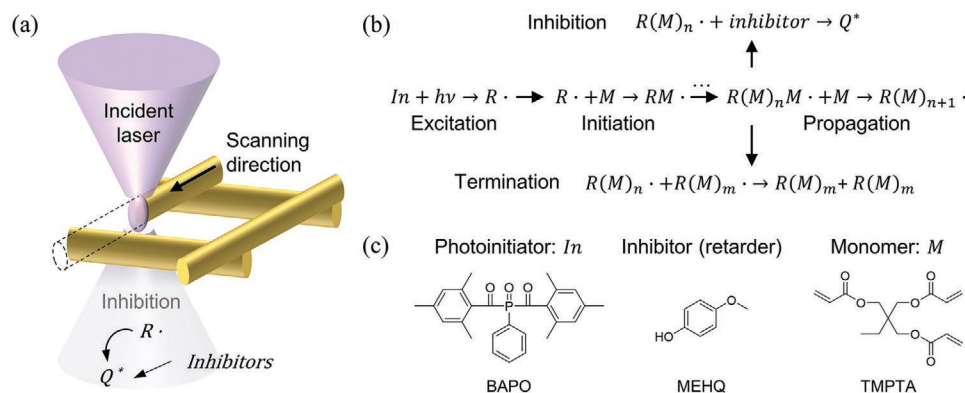


**Figure 1.** Experimental setup and nonlinear response working mechanism. a) Illustration of nonlinear 3D printing. b) Working mechanism of inhibition. In: photoinitiator, M: monomer, MEHQ: inhibitor,  $R\cdot$ : radical,  $Q^*$ : inert radical chain,  $R(M)_m$ : polymer. c) Chemical structures of the photoinitiator, monomer, and inhibitor used in the resin.

among the creation, diffusion, and consumption of initiation and inhibition species. The laser temporal modulation has three phases within each cycle. In phase I, the pulse starts, and radicals are generated to overcome local inhibition from inhibitors without polymer generated. Following in phase II with continuing irradiation, local inhibitors are nearly depleted while initiating radicals are still being generated to trigger polymerization. After the target feature is exposed (phase III), the laser power is tuned down and allows inhibition radicals to diffuse and recover for the next cycle/pulse. Ideally, minimum polymer chain diffusion would be favorable for high resolution and only inhibitors in this local position are used up, preventing extra polymer accumulation caused by the depletion of oxygen outside the writing region during the writing process. Considering the diffusivity of oxygen in the monomer is  $1.5 \times 10^{-9} \text{ m}^2 \text{ s}^{-1}$ , laser pulses of 10–100 ns kHz repetition rates, 2–5% duty cycles, and modulation contrast ratios around 10:1 are selected to allow oxygen to sufficiently refill around the writing voxel.<sup>[15,35,37]</sup> Using this selection of laser parameters, the diffusion length of oxygen is around 100 nm. This choice optimizes the usage of inhibition species to give a consistent writing performance. In a fresh resin, an initial threshold of 2.88 mW (all power levels in the following text are evaluated at the sample surfaces), corresponding to an average laser intensity of  $1.06 \text{ MW cm}^{-2}$  (all intensities are evaluated at the laser foci with more details in the supplementary information), was observed at a low scanning speed of  $100 \mu\text{m s}^{-1}$  (which is corresponding to  $690 \text{ voxel s}^{-1}$  or

a  $145 \text{ nm voxel size}$ ) and no polymerization was observed at lower laser powers. This threshold shows a drastic change in polymerization, indicating a high nonlinearity near this writing power where initiation starts to break its balance with inhibition during this dynamic writing process. As the power is increased to about 3.6 mW at the same  $100 \mu\text{m s}^{-1}$  speed, extra polymerizations can be observed as sharp features start to grow thicker. As we further increase power, initiating radicals overwhelm inhibiting radicals and dominate the process. In this high-power region, polymerization growth begins to approach a linear dependence of power.

An oxygen-rich environment can lead to a strong Schwarzschild-type nonlinearity that causes patterning distortion at the early stage, where the uncontrolled consumption of oxygen and inhibitor molecules could cause inconsistency and poor pattern definition in writing results. This undesired variation of the writing feature size could be sensitive near the writing threshold due to dose accumulation. **Figure 2** shows the pattern inconsistency caused by the Schwarzschild-type nonlinearity and our approach to resolve this issue. As shown in Figure 2a, an array of blocks with different average power and scanning speed is fabricated, where the first few blocks are incomplete due to the strong Schwarzschild effect. Figure 2b shows the stability of the writing process by using a constant average power to write an array of blocks under the Schwarzschild effect. As we can see, the strong inhibition in the background must be overcome before the actual writing can happen, and it causes the

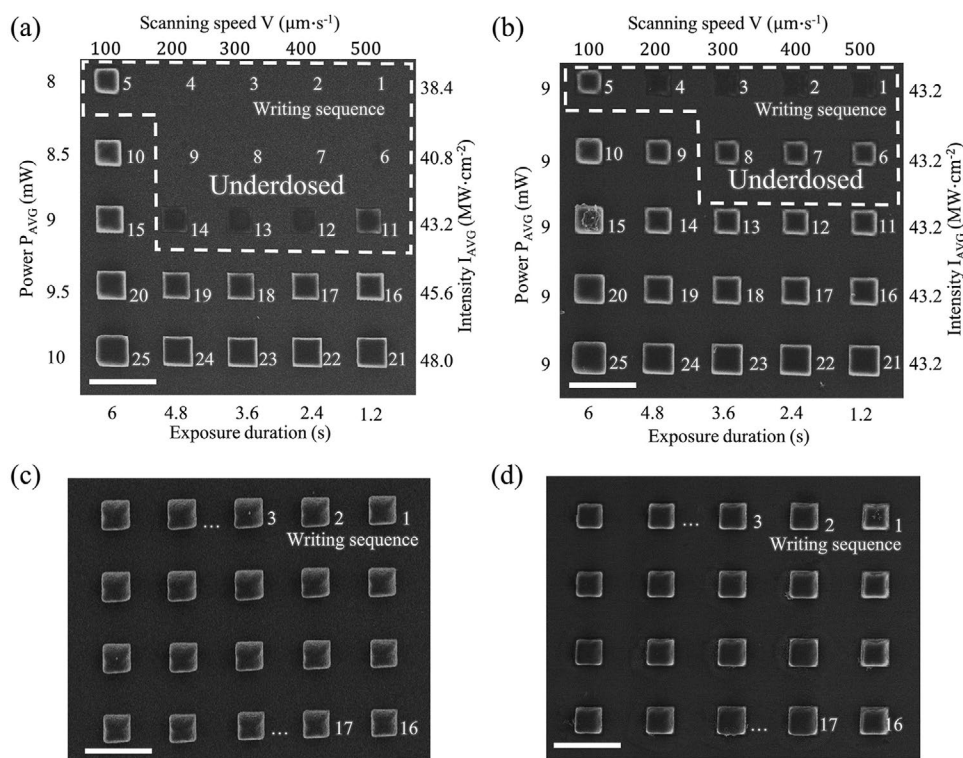


**Figure 2.** Nonlinearity characterization experiment and simulation. SEM images of arrays of block patterns under different writing conditions: a) Blocks printed for varying laser scanning speed and laser power. Scale bar:  $10 \mu\text{m}$ . b) Writing block pattern at constant average laser power and varying scanning speed, repeating five times with sequence of printing indicated. Scale bar:  $10 \mu\text{m}$ . c) A block array was fabricated by repeating the exposure 100 times (at a scanning speed of  $500 \mu\text{m s}^{-1}$  and average power of 1.8 mW.) Scale bar:  $10 \mu\text{m}$ . d) A block array fabricated after a pre-conditioning approach using a scanning speed of  $200 \mu\text{m s}^{-1}$  and an average power of 1.8 mW. (Pre-conditioning method: use a scanning speed of  $500 \mu\text{m s}^{-1}$  and average power of 1.08 mW to scan the area for 5 min before patterning.) Scale bar:  $10 \mu\text{m}$ .

incomplete polymerization of the blocks in the top row. However, once steady writing conditions are achieved, consistent blocks can be written uniformly after the second row with small variations. In Figure 2c, an array of blocks is created by repeatedly scanning the area for 100 rounds at a power level of 1.8 mW and a speed of  $500 \mu\text{m s}^{-1}$ , where the consistent blocks are written. Since the strong Schwarzschild effect is expected to fade away in the first few rounds, the fact that patterns are still well confined to the writing plane confirms that a strong nonlinearity still exists after repeated writings. This result also indicates that the strong Schwarzschild effect contributes significantly to the observed initial threshold (about 2.88 mW) and the required patterning threshold is about 1.8 mW without it. Therefore, we used a preconditioning method to establish a consistent writing environment by using a laser power level well below the threshold to repeatedly scan the area (a scanning speed of  $500 \mu\text{m s}^{-1}$  and an average power level of 1.08 mW to scan the area for 5 min) before starting patterning. Based on this preconditioning approach, consistent printing results are achieved with a 1.8 mW power level as shown in Figure 2d.

The effective order of nonlinearity in printing,  $\gamma$ , is usually characterized by using the relationship between the effective exposure dose rate,  $\dot{D}$ , which can be estimated by the amount of polymerization per unit time, and the incident laser power intensity  $I$  as  $\dot{D} \propto I^\gamma$  where  $\gamma = 2$  in a two-photon polymerization process. However, this method cannot be directly extended to characterize the order of nonlinearity for the one-photon polymerization process since the associated inhibition process is not directly determined by the laser intensity itself.<sup>[36]</sup> Instead, a different approach can be used to characterize nonlinearity by determining equivalent polymerization amounts at different pulse energies. To study this competing process, a multiphysics model is constructed to understand the intensity-dependent nonlinear response by capturing the laser light propagation, free-radical photopolymerization, and mass transport of participating materials, which are later compared with the exposure dose measurements. As shown in Figure S2 in the Supporting Information, the incident laser with pulsed intensity profile has a Gaussian spatial distribution, and it can generate initiating

radicals,  $R\cdot$ , by exciting the BAPO initiator.<sup>[38]</sup> The initiating radicals,  $R\cdot$ , react in three main paths including inhibition, chain-growth, and termination. Inhibition is the fastest reaction, with a reaction constant  $k_{O_2}$ , which is three to four orders of magnitude larger than the other two reactions.<sup>[39]</sup> The radicals and live chains preferably react with oxygen first and generate inert products, meaning that oxygen inhibition occurs before other reactions can happen. The second path, chain growth, is a temperature-sensitive process involving reactions of mixed chain lengths and molecule morphologies. Here we model it using Arrhenius's law with an equivalent activation energy and reaction constants for polymerization.<sup>[40,41]</sup> The termination reaction contains disproportionation and recombination of radicals. It has a high initial reaction rate which quenches radicals and decays as monomer conversion increases.<sup>[39,42]</sup> Here, the termination process is modeled using an empirical reaction rate with a dependence on conversion. In addition, the diffusion of the species also affects the local polymerization rate, particularly for that of oxygen whose diffusivity is more than two orders of magnitude higher than other species (monomers, initiators, radicals, ligaments, etc.).<sup>[15,43]</sup> The detailed parameters can be found in Table S1 in the Supporting Information.<sup>[15,39,42-45]</sup>

According to the simulated response under low laser power irradiation, the generated photoradicals and live chains mainly react with oxygen without initiating bulk polymerization. While oxygen is consumed locally, its concentration is partially maintained by in-bound diffusion from surroundings, whereas the refill of initiators is negligible due to their low diffusivity. Despite continuous laser irradiations for several seconds or even longer, the photoexcited reaction gradually stops since the initiators are eventually depleted at the laser focus. Under this condition, the local and neighboring oxygen concentrations may reduce significantly but remain sufficiently high to dominate in the overall reactions. If laser power increases beyond a threshold level for a prolonged period, the polymerization process starts to proceed as the neighboring oxygen concentration drops to a level where depletion of oxygen starts to occur locally at the laser focus. This delayed start of polymerization is referred to as the inhibition period.<sup>[46]</sup> Under intense laser irradiations, the oxygen will be

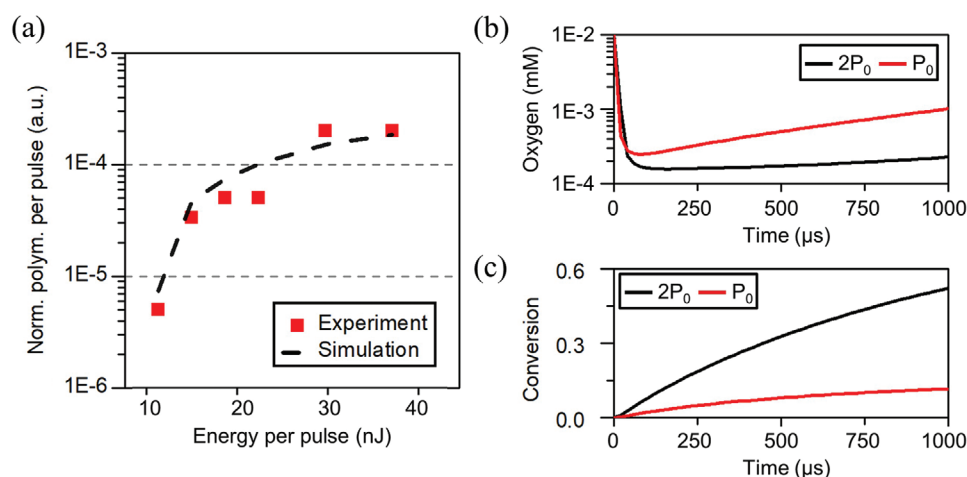


**Figure 3.** a) Minimum pulse energy required for polymerization in simulation/experiment. b) Simulation of oxygen consumption and c) simulation of monomer conversion for laser parameters  $P_0 = 2 \text{ mW}$ ,  $f = 100 \text{ kHz}$ , and duty cycle  $D = 10\%$ .

locally consumed before refill diffusion happens due to its low initial concentration and the newly generated radicals start to efficiently trigger the growth of polymer chains. The simulation captures the competing processes and predicts the formation of the nonlinear polymerization as a function of chemical concentrations and light intensity.

The multiphysics simulation results show good agreement with the trend of exposure dose measurements. The experiment was conducted to measure the polymerization amount per laser pulse through the minimum number of pulses required for fully polymerizing a dot. As shown in **Figure 3a**, no polymerization can be observed using pulse energies lower than 10 nJ (corresponding to an intensity level of  $0.40 \text{ MW cm}^{-2}$ ) for an exposure duration of 4.5 ms, indicating the existence of a threshold. When the pulse energy is near the threshold, the polymerization occurs and the polymerization amount per

pulse increases by more than ten times over a small power increase where a few thousand pulses are needed to generate a solid polymeric dot. The same trend of rapid change in polymerization amount can also be seen in the simulation.

**Figure 3b** shows the simulated intensity-dependent nonlinear responses at two laser powers  $P_0$  and  $2P_0$ , where  $P_0 = 2 \text{ mW}$  is near the writing threshold. For both cases, the oxygen is consumed within the first few laser pulses. The oxygen slowly recovers through diffusion when the laser power is low ( $P_0$ ), however remains depleted at a higher power level ( $2P_0$ ) which leads to increased conversion for polymerization. **Figure 3c** shows the evolution of monomer conversion under these two laser power levels, measured by the ratio of monomer consumed. A doubling of the power near the threshold can lead to over four times more conversion, which can solidify to form polymeric structures.

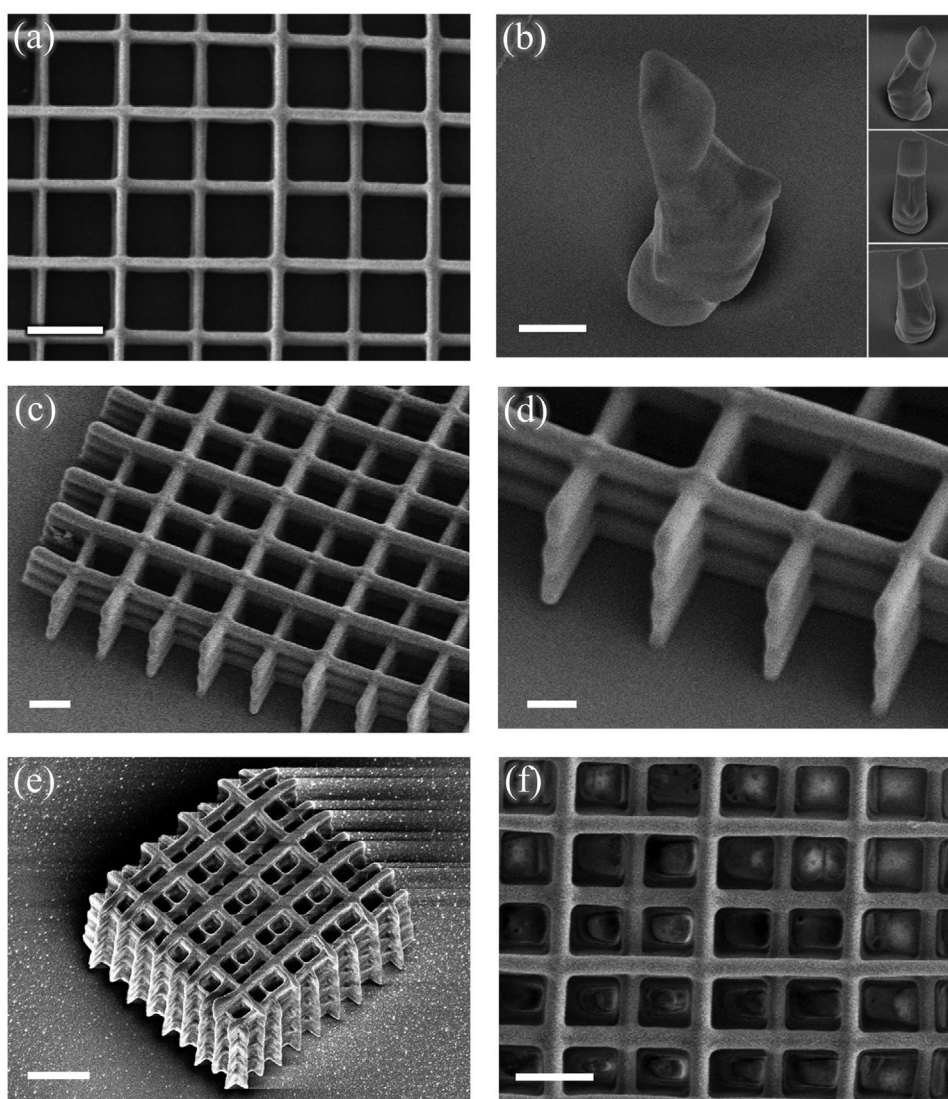


**Figure 4.** SEM images of fabricated structures. a) A single-layer fishnet structure. Scale bar:  $2 \mu\text{m}$ . b) A Moai statue from different angles. Scale bar:  $10 \mu\text{m}$ . c) A woodpile structure. Scale bar:  $2 \mu\text{m}$ . d) A zoomed-in view of (c). Scale bar:  $1 \mu\text{m}$ . e) A tall woodpile structure. Scale bar:  $5 \mu\text{m}$ . f) Top view of a woodpile structure. Scale bar:  $2 \mu\text{m}$ . For panel (a) and panels (c–f): scanning speed of  $50\text{--}100 \mu\text{m s}^{-1}$  and average power of  $1.8\text{--}2.88 \text{ mW}$ . For (b): scanning speed of  $1000 \mu\text{m s}^{-1}$  and average power of  $2.16 \text{ mW}$ .

**Figure 4a** shows a single-layer fishnet structure with a linewidth of 360 nm patterned by focusing the laser through a resin layer 160- $\mu\text{m}$  thick. Consistent writing without unwanted polymerization was achieved, with a resulting 360 nm linewidth. In addition, adding quenchers (Figure S3, Supporting Information), such as 4-hydroxy-2,2,6,6-tetramethylpiperidine 1-oxyl (TEMPO-OH), can effectively help to reduce the linewidth.<sup>[47,48]</sup> TEMPO-OH is a strong inhibition molecule and can be used to reduce the variation of the concentration of oxygen during printing. This effect is achieved at a molar concentration of TEMPO-OH 5% higher than the photoinitiator. Its thermal reversible initiation allows the fabrication of a smaller linewidth of 130 nm as shown in Figure S4a in the Supporting Information. Figure 4 panel b shows a Moai statue and panels c–f show 3D woodpile structures. The multiple individual layers can be observed with layer separation. The demonstrated feature sizes of the printed structure match the shape of the optical focus used in the experiments. The starting point of a written line tends to be slightly thinner due to local variations of inhibiting effect. By operating near the writing threshold, nanoscale solid structures can be written consistently under dynamic inhibition control. Figure S4b in the Supporting Information shows the finest feature sizes fabricated, including a suspended line of 130 nm thick using a laser power close to the writing threshold, which implies the possibility of printing sub-diffraction-limit features by trimming the voxel using engineered inhibition. Another demonstrated 3D printing result is shown in Figure S4c in the Supporting Information.

### 3. Conclusion

In conclusion, a 3D nanolithography method based on one-photon dosage-nonlinear polymerization is investigated using a compact 405 nm diode laser. By using a new dosage-nonlinear effect arising from the depletion of photoinitiators together with diffusion of inhibitors, a highly dosage-nonlinear polymerization process is achieved at high writing speed and low laser power. A modulated laser is used to optimize printing performance and achieve consistent nanoscale feature size. With this approach, complex structures are fabricated with the feature size of 100s of nm scale. A numerical model based on free radical polymerization reactions is studied to further understand the mechanism of this nonlinear polymerization. Compared to multiphoton lithography, this method used low-cost diode lasers with milliwatt scale power at a high scanning speed of 100s  $\mu\text{m s}^{-1}$ . These demonstrated results show potential to achieve fast one-photon 3D nanoscale fabrications through parallel operations and high writing speed.

### 4. Experimental Section

*Preparation of Resins:* All chemicals were purchased from Sigma-Aldrich, and they were used as received. The resin in which the microstructures were directly written was mixed using the components described as follows. The monomer mixture was composed of 95 wt% trimethylolpropane triacrylate (TMPTA) or pentaerythritol triacrylate (PETA) and 5 wt% of triethylene glycol dimethacrylate (TEGDMA). This composition allowed for quantification of the different rates of

crosslinking of the monomers to reduce undesired polymerization outside of the voxel. Phenylbis(2,4,6-trimethylbenzoyl) phosphine oxide (BAPO) was later added as the photoinitiator with a concentration of 80 ppm in the monomer mixture. Also, 0.3 wt% of 4-methoxyphenol (MEHQ) was added as the inhibitor, and 0.1 wt% of 1-(phenyldiazenyl) naphthalen-2-ol (Sudan I) was added as the photoabsorber. All the materials were measured and mixed and sonicated for 2 hours in the open air and stored in a vial under room temperature with minimum exposure to ambient light. Due to the concentration of Sudan I compared to other species, the absorption spectrum of the resin was almost the same as Sudan I.

*Direct Laser Writing:* As shown in Figure S1 in the Supporting Information, a system was constructed for laser scanning experiments with a compact diode laser operating at 405 nm wavelength. A spatial filter aperture was integrated into the laser path to refine the beam quality. To scan the beam laterally, the laser was steered by a piezo scanning mirror to provide the in-plane 2D motions. An objective z-piezo stage was mounted under the objective to actuate the focal plane in the z-direction and therefore a 3D patterning space can be accessed. An oil immersion no cover glass (NCG) objective lens with a numerical aperture of 1.4 and 100 $\times$  magnification was mounted on the z-piezo stage. A drop of resin was placed between the objective and a cover slide to conduct the patterning experiments.

### Supporting Information

Supporting Information is available from the Wiley Online Library or from the author.

### Acknowledgements

This work was supported by the National Science Foundation (NSF) through the Scalable Nanomanufacturing Program (Award Number: 1634832, Program Manager: Dr. Khershed Cooper), and the NSF is thanked for their gracious support. Dr. Jin Cui and Bojing Yao are thanked for their helpful discussions.

### Conflict of Interest

The authors declare no conflict of interest.

### Data Availability Statement

The data that supports the findings of this study are available in the supplementary material of this article.

### Keywords

3D printing, additive manufacturing, direct laser writing, one-photon polymerization

Received: October 21, 2021

Published online:

[1] I. Gibson, D. W. Rosen, B. Stucker, *Additive Manufacturing Technologies*, Springer, Berlin 2014.

[2] M. Vaezi, H. Seitz, S. Yang, *Int. J. Adv. Manuf. Technol.* **2013**, *67*, 1721.

- [3] O. Diegel, A. Nordin, D. Motte, *Additive Manufacturing Technologies*, Springer, Berlin **2019**.
- [4] W. Gao, Y. Zhang, D. Ramanujan, K. Ramani, Y. Chen, C. B. Williams, C. C. L. Wang, Y. C. Shin, S. Zhang, P. D. Zavattieri, *Comput. Des.* **2015**, 69, 65.
- [5] W. E. Frazier, *J. Mater. Eng. Perform.* **2014**, 23, 1917.
- [6] A. N. Dickson, J. N. Barry, K. A. McDonnell, D. P. Dowling, *Addit. Manuf.* **2017**, 16, 146.
- [7] A. Vyatskikh, S. Delalande, A. Kudo, X. Zhang, C. M. Portela, J. R. Greer, *Nat. Commun.* **2018**, 9, 593.
- [8] L. R. Meza, S. Das, J. R. Greer, *Science* **2014**, 345, 1322.
- [9] D. Gailevičius, V. Padolskytė, L. Mikoliūnaitė, S. Šakirzanovas, S. Juodkazis, M. Malinauskas, *Nanoscale Horiz.* **2019**, 4, 647.
- [10] C. Xia, Ph.D. Thesis, University of Illinois at Urbana-Champaign, **2010**.
- [11] D. A. Walker, J. L. Hedrick, C. A. Mirkin, *Science* **2019**, 366, 360.
- [12] J. R. Tumbleston, D. Shirvanyants, N. Ermoshkin, R. Januszewicz, A. R. Johnson, D. Kelly, K. Chen, R. Pinschmidt, J. P. Rolland, A. Ermoshkin, *Science* **2015**, 347, 1349.
- [13] M. P. De Beer, H. L. Van Der Laan, M. A. Cole, R. J. Whelan, M. A. Burns, T. F. Scott, *Sci. Adv.* **2019**, 5, eaau8723.
- [14] B. E. Kelly, I. Bhattacharya, H. Heidari, M. Shusteff, C. M. Spadaccini, H. K. Taylor, *Science* **2019**, 363, 1075.
- [15] M. Shusteff, A. E. M. Browar, B. E. Kelly, J. Henriksson, T. H. Weisgraber, R. M. Panas, N. X. Fang, C. M. Spadaccini, *Sci. Adv.* **2017**, 3, eaao5496.
- [16] S. Maruo, O. Nakamura, S. Kawata, *Opt. Lett.* **1997**, 22, 132.
- [17] B. H. Cumpston, S. P. Ananthavel, S. Barlow, D. L. Dyer, J. E. Ehrlich, L. L. Erskine, A. A. Heikal, S. M. Kuebler, I.-Y. S. Lee, D. McCord-Maughon, *Nature* **1999**, 398, 51.
- [18] E. Skliutas, M. Lebedevaite, E. Kabouraki, T. Baldacchini, J. Ostrauskaite, M. Vamvakaki, M. Farsari, S. Juodkazis, M. Malinauskas, *Nanophotonics* **2021**, 10, 1211.
- [19] P. Kiefer, V. Hahn, M. Nardi, L. Yang, E. Blasco, C. Barner-Kowollik, M. Wegener, *Adv. Opt. Mater.* **2020**, 8, 2000895.
- [20] J. Fischer, M. Wegener, *Opt. Mater. Express* **2011**, 1, 614.
- [21] T. L. Andrew, H.-Y. Tsai, R. Menon, *Science* **2009**, 324, 917.
- [22] S. Juodkazis, V. Mizeikis, K. K. Seet, M. Miwa, H. Misawa, *Nanotechnology* **2005**, 16, 846.
- [23] L. Jonušauskas, D. Gailevičius, S. Rekštytė, T. Baldacchini, S. Juodkazis, M. Malinauskas, *Opt. Express* **2019**, 27, 15205.
- [24] S. K. Saha, D. Wang, V. H. Nguyen, Y. Chang, J. S. Oakdale, S.-C. Chen, *Science* **2019**, 366, 105.
- [25] V. Hahn, P. Kiefer, T. Frenzel, J. Qu, E. Blasco, C. Barner-Kowollik, M. Wegener, *Adv. Funct. Mater.* **2020**, 30, 1907795.
- [26] T. Zandrini, O. Shan, V. Parodi, G. Cerullo, M. T. Raimondi, R. Osellame, *Sci. Rep.* **2019**, 9, 11761.
- [27] C. Maibohm, O. F. Silvestre, J. Borme, M. Sinou, K. Heggarty, J. B. Nieder, *Sci. Rep.* **2020**, 10, 8740.
- [28] S. Maruo, K. Ikuta, *Appl. Phys. Lett.* **2000**, 76, 2656.
- [29] S. Maruo, K. Ikuta, *Sens. Actuators, A* **2002**, 100, 70.
- [30] P. Delrot, D. Loterie, D. Psaltis, C. Moser, *Opt. Express* **2018**, 26, 1766.
- [31] T. F. Scott, B. A. Kowalski, A. C. Sullivan, C. N. Bowman, R. R. McLeod, *Science* **2009**, 324, 913.
- [32] Z. Gan, Y. Cao, R. a Evans, M. Gu, *Nat. Commun.* **2013**, 4, 2061.
- [33] M. Thiel, J. Fischer, G. Von Freymann, M. Wegener, *Appl. Phys. Lett.* **2010**, 97, 221102.
- [34] M. T. Do, T. T. N. Nguyen, Q. Li, H. Benisty, I. Ledoux-Rak, N. D. Lai, *Opt. Express* **2013**, 21, 20964.
- [35] Q. C. Tong, D. T. T. Nguyen, M. T. Do, M. H. Luong, B. Journet, I. Ledoux-Rak, N. D. Lai, *Appl. Phys. Lett.* **2016**, 108, 183104.
- [36] N. Liaros, J. T. Fourkas, *Opt. Mater. Express* **2019**, 9, 3006.
- [37] P. Mueller, M. Thiel, M. Wegener, *Opt. Lett.* **2014**, 39, 6847.
- [38] A. Eibel, D. E. Fast, G. Gescheidt, *Polym. Chem.* **2018**, 9, 5107.
- [39] R. Li, F. J. Schork, *Ind. Eng. Chem. Res.* **2006**, 45, 3001.
- [40] A. M. van Herk, *Macromol. Rapid Commun.* **2009**, 30, 1964.
- [41] S. Laki, A. A. Shamsabadi, H. Riazi, M. C. Grady, A. M. Rappe, M. Soroush, *Ind. Eng. Chem. Res.* **2019**, 59, 2621.
- [42] D. S. Achilias, *Macromol. Theory Simul.* **2007**, 16, 319.
- [43] R. Parthasarathy, A. Misra, J. Park, Q. Ye, P. Spencer, *J. Mater. Sci. Mater. Med.* **2012**, 23, 1157.
- [44] M. G. Neumann, W. G. Miranda Jr, C. C. Schmitt, F. A. Rueggeberg, I. C. Correa, *J. Dent.* **2005**, 33, 525.
- [45] M. Bouzrati-Zerelli, J. Kirschner, C. P. Fik, M. Maier, C. Dietlin, F. Morlet-Savary, J. P. Fouassier, J.-M. Becht, J. E. Klee, J. Lalevée, *Macromolecules* **2017**, 50, 6911.
- [46] H. Becker, H. Vogel, *Chem. Eng. Technol.* **2006**, 29, 1227.
- [47] K. M. T. Stengle, L. W. Shacklette, L. Eldada, J. T. Yardley, C. Xu, S. M. Zimmerman, K. A. Horn, (Corning Inc.), *US6162579*, **2000**.
- [48] G. Pan, E. D. Sudol, V. L. Dimonie, M. S. El-Aasser, *J. Polym. Sci. Part A Polym. Chem.* **2004**, 42, 4921.
- [49] H. Fischer, *Macromolecules* **1997**, 30, 5666.